STRUCTURE FUNCTIONS AND THE TRANSITION REGION FROM PHOTOPRODUCTION TO DEEP INELASTIC SCATTERING

DORIAN KCIRA
University of Wisconsin
ZEUS/DESY
Notkestrasse 85
22607 Hamburg
GERMANY
E-mail: dorian.kcira@desy.de

Precise inclusive and dijet measurements are presented that extend the kinematic domain of HERA and cover the transition region from deep inelastic scattering to photoproduction. The rise of the structure function F_2 at low x persists but is shallower at lower Q^2. Dijet measurements can significantly constrain the parton distribution functions of the virtual photon.

1. Introduction

In deep inelastic *ep* scattering (DIS) at HERA, a photon of negative squared momentum (virtuality, Q^2) is exchanged. The highly virtual pointlike photon is used as a probe and precise determinations of proton structure are performed by inclusive measurements. Measurements of jet cross sections in DIS provide further information, are sensitive to the proton structure and allow precise tests of perturbative QCD (pQCD).

In photoproduction ($Q^2 \simeq 0$), the requirement of events with high transverse energy jets provides for a hard scale in the interaction and allows comparison to pQCD calculations. In photoproduction the measurements are sensitive to both the structure of the proton and the structure of the (quasi-real) photon.

Both the DIS and photoproduction regimes have been extensively studied at HERA and pQCD predictions have been successful in describing the data. The physical picture and the language used in the two regimes is not the same. Therefore, data and predictions in the region between them are particularly interesting.

Until recently, not much data had been gathered at HERA in the transition region between DIS and photoproduction mainly because of the experimental difficulty of identifying the scattered lepton at small scattering angles. Recently, the H1 and ZEUS Collaborations have performed measurements that "scan" this region using inclusive and dijet events. It must be noted that these are conceptually two different ways of crossing the transition region. In the case of inclusive measurements the transition is from a hard regime (DIS, with hard scale Q^2) to a soft regime (photoproduction). In the case of dijet measurements the requirement of high transverse energy jets allows application of pQCD throughout the transition from real ($Q^2 \simeq 0$) photons, which can have structure, to virtual pointlike photons. In this second transition two hard scales play a role: Q and E_T, the transverse energy scale of the jets. Depending on the interplay of these two hard scales, the photon may or may not display a structure. Both these types of measurements are presented in this paper.

2. Inclusive Measurements

Measurements of the proton structure function F_2 in the region of $Q^2 \gg 1$ GeV^2 have shown a good description of the data by perturbative QCD (pQCD) [1,2,3]. On the other hand the region $Q^2 < 1$ GeV^2 is described by models based on generalized vector meson dominance [4] and Regge theory [5]. Therefore, the region of Q^2 around 1 GeV^2 deserves particular attention.

In this section the latest HERA measurements in the transition region from low to high Q^2 are presented together with comparisons to perturbative and non-perturbative approaches. These measurements use different experimental techniques for accessing the low Q^2 data, which are reflected in the titles of the subsections.

2.1. *Initial State Radiation Analysis*

Events with QED initial state radiation (ISR) have been used to measure F_2. The measurement is based on the data taken during 1996 with the ZEUS detector (3.78 pb^{-1}) [6]. The emission of a hard photon from the initial-state positron leads to a reduction in the center-of-mass energy of the hard scattering particles. This means that lower values of Q^2 can be accessed.

The F_2 measurements are shown in Fig. 1 (left plot) as a function of x at different values of Q^2 together with the most recently published F_2 measurements [7,8] and the BPC/BPT [9] results. The data sets are in good

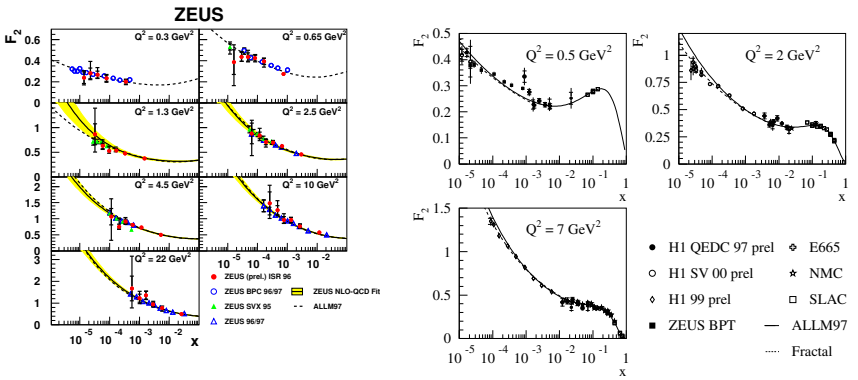

Figure 1. Left plot: F_2 versus x for fixed Q^2. The results of the ISR analysis are shown together with previously published ZEUS results. The yellow band shows the predictions from the ZEUS NLO QCD fit while the dashed curve those from ALLM97. Right plot: F_2 measurement from QEDC analysis (closed circles) compared with other HERA and fixed target measurements. The solid line is the prediction from the ALLM97 parametrization while the dashed line represents the fractal fit, plotted for $y > 0.0003$.

agreement in the region of overlap, completing the coverage of the x-Q^2 plane at low Q^2. The results are compared to the predictions of the ZEUS NLO QCD fit for $Q^2 \geq 1.3$ GeV^2 and to the predictions of ALLM97 [10] over the whole Q^2 range. Both predictions give a good description of the data.

2.2. *QED Compton Analysis*

The H1 Collaboration has performed measurements of F_2 using QED Compton scattering events[11]. The measurements use e^+p data with an integrated luminosity of 9.25 pb^{-1} collected during 1997.

The QED Compton process corresponds to low Q^2 and a large virtual electron mass. The final state topology is given by an azimuthal back-to-back configuration of the outgoing positron and photon detected under rather large scattering angles. Their transverse momenta balance such that very low values of Q^2 are experimentally accessible.

The F_2 values measured in QED Compton scattering are depicted in Fig. 1 (right plot) as a function of x at fixed Q^2 and compared to other HERA and fixed target data. The kinematic range is extended at very low Q^2 towards higher x values, complementing the standard inclusive and shifted vertex measurements. The results overlap with the region measured in fixed target experiments. Good agreement is observed.

2.3. *Shifted Vertex Analysis*

A special run was performed in 2000 at HERA in which the interaction vertex was shifted towards the proton beam direction by 70 cm. This increased the acceptance for positrons with smaller scattering angles. This again allows lower values of Q^2 to be accessed. The data presented here[12] correspond to an integrated luminosity of 0.6 pb^{-1}, a factor of four larger than the previous shifted vertex data samples at H1[13] and ZEUS [8]. The combination of larger statistics and the new Backward Silicon Tracker (BST) allowed the H1 Collaboration to make measurements with higher precision than previously.

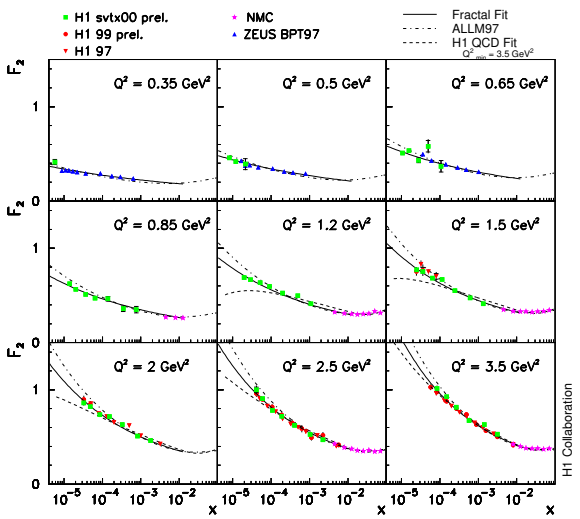

Figure 2. F_2 from H1 shifted vertex data (squares), H1 99 and 97 nominal vertex data (points and triangles), larger x data from BPC/BPT (triangles) and from NMC (stars).

In Fig. 2 the F_2 data are compared with phenomenological predictions obtained from fits to previous data. The best description is given by the fractal model parametrization [14] (solid curve) the parameters of which were determined by fitting the ZEUS BPC/BPT data and the published low Q^2 H1 data [1]. The ALLM97 parametrization (dashed-dotted curves) similarly used previous data which leads to an acceptable description of the present F_2 data with a slightly stronger rise with decreasing x for $Q^2 \geq 1$ GeV^2

than is observed in the H1 data. The prediction from the H1 NLO QCD fit [1] is also shown (dashed curves). This fit only included data with $Q^2 \geq 3.5$ GeV^2. Its backward extrapolation undershoots measurements at lower Q^2. At $Q^2 \leq 1$ GeV^2 the strong coupling constant $\alpha_S(Q^2)$ becomes large, making a comparison with NLO QCD meaningless.

In Fig. 3 (left plot) the photon-proton cross section, $\sigma_{\gamma^* p}$, which is proportional to F_2/Q^2, is plotted as a function of Q^2 at different values of $W^2 \simeq sy$. W is the invariant mass of the $\gamma^* p$ system. The new data fill the gap between previous measurements at lower and higher Q^2 and reach similar accuracy. The same three parametrizations are plotted as in Fig. 2. At $Q^2 \simeq 1$ GeV^2 the ALLM97 parametrization is too large at high W and the QCD fit fails, as expected. For $Q^2 \to 0$, the fractal model fit is too steep to describe the total photoproduction cross section (not shown here). However, this could be cured by considering mass effects in the fractal Ansatz [15].

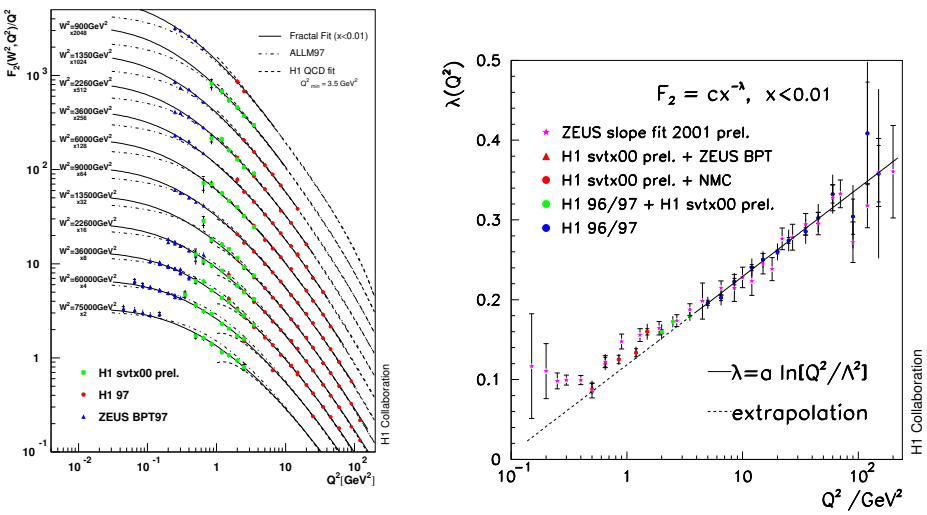

Figure 3. Left plot: measurements of the structure function F_2 represented as F_2/Q^2 compared to the Fractal fit, H1 QCD fit and the ALLLM97 parametrization. Right plot: determination of the exponent $\lambda(x, Q^2)$ from fits to F_2 as measured from H1 and ZEUS. The straight line represents a linear fit to the measurements for $Q^2 \geq 3.5$ GeV^2.

2.4. *The Rise of F_2 at low x*

To quantify the behaviour of the rise of F_2 towards low x at fixed Q^2 the H1 and ZEUS Collaborations have measured the derivative:

$$\left(\frac{\partial \ln F_2(x,Q^2)}{\partial \ln x}\right) \equiv -\lambda(Q^2)$$

Using the data presented in this paper, the measurement of $\lambda(Q^2)$ is extended to the transition region as plotted in Fig. 3 (right plot). For values $Q^2 < 1$ GeV^2 the derivative $\lambda(Q^2)$ is seen to significantly deviate from an extrapolation of the linear behaviour determined from the data in the deep inelastic scattering region ($Q^2 \geq 3.5$ GeV^2). From soft hadronic interaction models, it is expected that for $Q^2 \to 0$, $\lambda \to 0.08$. HERA data agree with these expectations.

3. Dijet Measurements

It has been established that the real photon ($Q^2 \simeq 0$) has a partonic structure [16]. In contrast, in hard collisions at high Q^2 the photon is considered to be pointlike. In leading order (LO) QCD two types of processes contribute to jet photoproduction: direct, in which the photon couples as a pointlike particle to quarks in the hard scatter; and resolved, in which the photon acts as a source of partons. Both processes lead to two jets in the final state. The $x_\gamma^{\rm obs}$ variable:

$$x_\gamma^{\rm obs} = \frac{\sum_{\rm jets}(E^{\rm jet} - p_z^{\rm jet})}{\sum_{\rm hadrons}(E - p_z)} \ ,$$

which measures the fraction of the photon momentum participating in the production of the dijet system, is used to separate the two processes since resolved (direct) processes dominate at low (high) $x_\gamma^{\rm obs}$ values [17]. In the above definition the upper sum runs over the two jets with highest transverse energy and the lower sum runs over all final state hadrons in the laboratory frame.

Within fixed-order QCD, only pointlike photon interactions are expected to contribute to jet production in DIS. However, two scales play a role in the interaction: Q and the jet transverse energy, $E_T^{\rm jet}$. QCD predicts that for high Q^2 ($Q^2 \gg (E_{\rm T}^{\rm jet})^2$) the photon will behave as a pointlike particle. For $Q^2 \ll (E_{\rm T}^{\rm jet})^2$ the photon may present a partonic structure, even for relatively large values of Q^2, which is resolved at a scale related

to the transverse energy of the jets. Therefore, resolved processes may contribute significantly to the total cross section.

Dijet measurements in photoproduction, DIS and the transition region are presented in this section. Different LO and NLO pQCD calculations are compared with the data.

The H1 Collaboration has measured dijet cross sections in the $\gamma^* p$ center-of-mass frame using a sample of 16.3 pb^{-1} data collected in 1999[18]. The phase space is defined by: $2 < Q^2 < 80$ GeV^2, the inelasticity $0.1 < y < 0.85$, the transverse energy of the two leading jets $E_{\mathrm{T}}^{\mathrm{jet1,2}} > 5$ GeV, $\overline{E}_{\mathrm{T}} = (E_{\mathrm{T}}^{\mathrm{jet1}} + E_{\mathrm{T}}^{\mathrm{jet2}})/2 > 6$ GeV and the pseudorapidity of the two leading jets $-2.5 < \eta^{\mathrm{jet1,2}} < 0$.

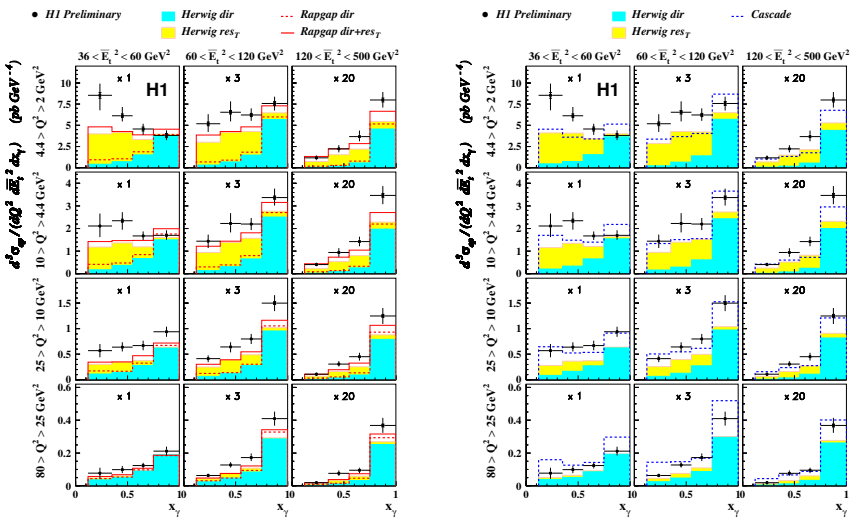

Figure 4. Triple differential cross section as a function of x_γ^{obs}, $\overline{E}_{\mathrm{T}}^2$ and Q^2. The data are compared to HERWIG and RAPGAP MC predictions (left plot). Separately shown are the components of the cross section from direct (dir) and resolved γ^*. Predictions of the HERWIG and CASCADE MC are also compared to the data (right plot).

The triple differential dijet cross sections measured as a function of Q^2, $\overline{E}_{\mathrm{T}}^2$, and x_γ^{obs} are shown in Fig. 4. The prediction of HERWIG [19] and RAPGAP [20] Monte Carlo (MC) simulations with the SaS 1D[21] parametrization of the virtual photon parton distribution function (PDF), as well as the pure direct contributions are compared to the data in Fig. 4 (left plot). In general HERWIG and RAPGAP tend to underestimate the measured

cross sections. The direct contributions reasonably describe the data in the highest Q^2 bin, while a clear need for resolved processes is observed for $Q^2 \ll \overline{E}_{\rm T}^2$. The measured cross sections are compared in Fig. 4 (right plot) to the predictions of the CASCADE [22] MC program, which uses the CCFM evolution scheme. This theoretical approach is based on non-k_T-ordered parton cascades and does not include the concept of virtual photon structure. CASCADE describes the data reasonably well but not perfectly.

The ZEUS Collaboration has studied the dependence of dijet production on Q^2 by measuring dijet cross sections in the range $0 \lesssim Q^2 < 2000$ GeV^2 using the 1996-1997 data sample[23], which corresponds to an integrated luminosity of 38.6 pb^{-1}. Inclusive dijet cross sections were measured for jets with transverse energy $E_T^{1,2} > 7.5, 6.5$ GeV and pseudorapidities in the photon-proton center-of-mass frame in the range $-3 < \eta^{\rm jet} < 0$.

Fig. 5 presents the differential dijet cross section, $d\sigma/dQ^2$, for the direct-enhanced region ($x_\gamma^{\rm obs} > 0.75$) and the resolved-enhanced region ($x_\gamma^{\rm obs} < 0.75$) together with the total dijet cross section. The measurements are precise and cover a wide range of photon virtualities, including the transition region from photoproduction to DIS. As expected, the cross section for $x_\gamma^{\rm obs} < 0.75$ falls more rapidly than that for $x_\gamma^{\rm obs} > 0.75$. Even though the dijet cross section is dominated by interactions with $x_\gamma^{\rm obs} > 0.75$ for $Q^2 \gtrsim 10$ GeV^2, there is still a contribution of approximately 24% from low-$x_\gamma^{\rm obs}$ events even for Q^2 as high as 500 GeV^2. The NLO QCD calculations of DISASTER++ [24] with $\mu_R^2 = Q^2 + (E_T^{\rm jet})^2$ are compared to the measurements. The photoproduction measurement is compared with the NLO prediction from Frixione and Ridolfi where E_T^2 is used as the scale. The measured cross section for $x_\gamma^{\rm obs} > 0.75$ is reasonably well described by the calculation but the measured cross section for $x_\gamma^{\rm obs} < 0.75$ is significantly underestimated for high Q^2.

Fig. 6 shows the ratio $R = \frac{{\rm d}\sigma}{{\rm d}Q^2}(x_\gamma^{\rm obs} < 0.75)/\frac{{\rm d}\sigma}{{\rm d}Q^2}(x_\gamma^{\rm obs} > 0.75)$ as a function of Q^2 in three different regions of $\overline{E}_T^2$. The Q^2 dependence of the data is stronger at low $\overline{E}_T^2$ than at higher $\overline{E}_T^2$, showing that the low $x_\gamma^{\rm obs}$ component is suppressed at low Q^2 as $\overline{E}_T^2$ increases and vice-versa. Predictions from HERWIG assuming the SaS 1D and GRV[25] parametrizations of the photon PDFs are compared to the data in Fig. 6 (left plot). The SaS 1D parametrization contains the suppression of the virtual photon structure with increasing virtuality. The predictions fall with increasing Q^2 and reproduce the fall of the data relatively well. On the other hand the predictions using GRV which assumes no suppression of the virtual photon

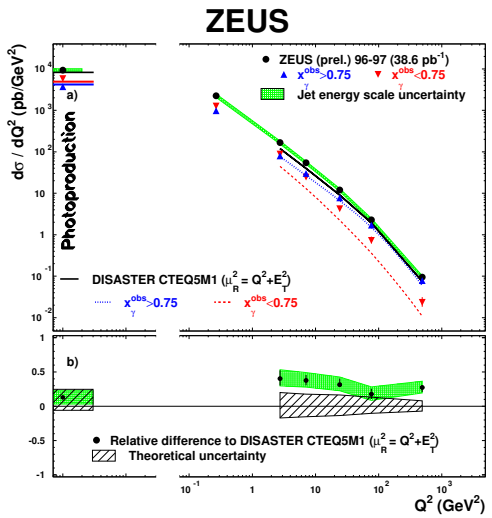

Figure 5. a) Measured dijet cross-sections $d\sigma/dQ^2$ for $x_\gamma^{\rm obs} > 0.75$ (upwards triangles) $d\sigma/dQ^2$ for $x_\gamma^{\rm obs} < 0.75$ (downwards triangles) and $d\sigma/dQ^2$ for the whole $x_\gamma^{\rm obs}$ region (black dots). The shaded band represents the uncertainty in the absolute energy scale of the jets. The NLO QCD calculations of DISASTER++ ($\mu_R^2 = Q^2 + (E_T^{\rm jet})^2$) and Frixione ($\mu_R^2 = (E_T^{\rm jet})^2$) are shown for each cross-section. b) Relative difference of the measured cross-section to the DISASTER++ and Frixione calculations. The hatched band shows the theoretical uncertainty of the calculations.

structure, are relatively constant at the level of the photoproduction ratio of the data. The NLO calculations are compared to the data in Figure 6 (right plot). For photoproduction, the calculations lie below the data for all $\overline{E}_T^2$. The NLO-prediction which used GRV for the photon PDFs is closer to the data than the one using AFG [26]. However, they underestimate the relative cross section at low $x_\gamma^{\rm obs}$. The DISASTER++ predictions show some suppression of the low $x_\gamma^{\rm obs}$ contribution with increasing Q^2, however they underestimate the proportion of low $x_\gamma^{\rm obs}$ relative to high $x_\gamma^{\rm obs}$.

4. Summary and Conclusions

New precise measurements of the structure function F_2 have been performed extending the kinematic domain of HERA and covering the transition region from DIS to photoproduction. The data are in agreement with the previous HERA data at higher and lower Q^2 and those from fixed targed experiments in the region of overlap.

Differential dijet cross sections have been measured in a large range of

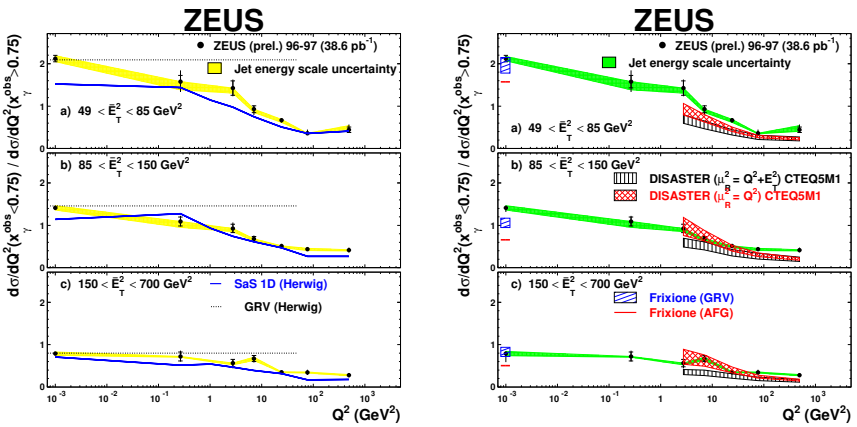

Figure 6. Measured ratio $R = \frac{d\sigma}{dQ^2}(x_\gamma^{\rm obs} < 0.75)/\frac{d\sigma}{dQ^2}(x_\gamma^{\rm obs} > 0.75)$ as a function of Q^2 in different regions of $\overline{E}_T^2$ (black dots). The LO calculations of HERWIG with using the SaS 1D and GRV photon pdfs (left plot) as well as the NLO predictions from DISASTER++ and Frixione-Ridolfi (right plot) are also shown.

photon virtualities, including the transition region from photoproduction to DIS. The data are reasonably well described by DGLAP LO models which introduce virtual photon structure, suppressed with increasing Q^2. The non-k_T-ordered CCFM-based approach also does a relatively good job in describing the measurements. These data have the potential to significantly constrain virtual photon PDFs and should be taken into account in future fits. The currently available NLO QCD calculations have large uncertainties at low Q^2, where the presence of the resolved photon contribution is expected. Improved higher-order or resummed calculations are needed. The NLO QCD predictions generally underestimate the cross section at low $x_\gamma^{\rm obs}$ relative to that of high $x_\gamma^{\rm obs}$.

References

1. H1 Collaboration, C. Adloff et al., *Eur. Phys. J.* **C 21**, 33 (2001), [hep-ex/0012053].
2. H1 Collaboration, C. Adloff et al., *Eur. Phys. J.* **C 30**, 1 (2003).
3. ZEUS Collaboration, S. Chekanov et al., *Phys. Rev.* **D 67**, 012007 (2003).
4. J.J. Sakurai and D. Schildknecht, *Phys. Lett.* **B 40**, 121 (1972).
5. P.D.B. Collins, *An Introduction to Regge Theory and High Energy Scattering*, Cambridge University Press (1977).
6. ZEUS Collaboration, *Measurement of the proton structure functions* F_2 *and*

F_L *using initial state radiative events at HERA*, **EPS 2003 Conference**, Abstract 502 (2003).
7. ZEUS Collaboration, S. Chekanov et al., *Eur. Phys. J.* **C 21**, 443 (2001).
8. ZEUS Collaboration, J. Breitweg et al., *Eur. Phys. J.* **C 7**, 609 (1999).
9. ZEUS Collaboration, J. Breitweg et al., *Phys. Lett.* **B 487**, 53 (2000).
10. H. Abramowitz and A. Levy, *DESY 97-251* (1997).
11. H1 Collaboration, *Measurement of the Proton Structure Function* F_2 *at low* Q^2 *in QED Compton Scattering at HERA*, **EPS 2003 Conference**, Abstract 084 (2003).
12. H1 Collaboration, *Measurement of the Inclusive Deep Inelastic Scattering Cross Section at* $Q^2 \simeq 1$ GeV^2 *with the H1 Experiment*, **EPS 2003 Conference**, Abstract 082 (2003).
13. H1 Collaboration, C. Adloff et al., *Nucl. Phys.* **B 497**, 3 (1997).
14. T. Lastovicka, Self-similar Properties of the Proton Structure at low x *Eur. Phys. J.* **C** , to appear, [hep-ph/0203260] (2002).
15. T. Lastovicka, in "DIS 2002 - 10th Int. Workshop on Deep Inelastic Scattering", to appear in *Acta Phys. Polonica* **B**
16. PLUTO Collaboration, C. Berger et al., *Nucl. Phys.* **B 281**, 365 (1987).
17. ZEUS Collaboration, M. Derrick et al., *Phys. Lett.* **B 322**, 287 (1994).
18. H1 Collaboration, *Measurement of Dijet Cross-Sections at Low* Q^2 *at HERA*, **EPS 2003 Conference**, Abstract 085 (2003).
19. G. Marchesini et al., HERWIG: A Monte Carlo Event Generator for Simulating Hadron Emission Reactions With Interfering Gluons, Comp. Phys. Comm. **67**, 465 (1992).
20. H. Jung, *Hard Diffractive Scattering in High Energy ep Collisions and the Monte Carlo Generator* RAPGAP, Comp. Phys. Comm. **86**, 147 (1995).
21. G.A. Schuler and T. Sjöstrand, *Parton Distributions of the Virtual Photon*, *Phys. Lett.* **B 376**, 193 (1996).
22. H. Jung and G. P. Salam, *Hadronic Final State Predictions from CCFM: The Hadron-Level Monte Carlo Generator* CASCADE, *Eur. Phys. J.* **C 19**, 351 (2001).
23. ZEUS Collaboration, *The* Q^2 *Dependence of Dijet Production at HERA*, **EPS 2003 Conference**, Abstract 585 (2003).
24. D. Graudenz, *DISASTER++ Version 1.0*, hep-ph/9710244, (1997).
25. M. Glück, E. Reya and A. Vogt, *Photonic Parton Distributions*, *Phys. Rev.* **D 46**, 1793 (1992).
26. P. Aurenche, J.P. Guillet and M. Fontannaz, *Parton Distributions in the Photon*, Z. Phys. **C 64**, 621 (1994).